IAC-19/A6/9x50602

# Analysing the Correlation Performance of ESA's Planned Space-based GEO Surveillance Mission

Benedikt Reihs[1,*], Alessandro Vananti[1], Jan Siminski[2], Tim Flohrer[3], and Thomas Schildknecht[1]

[1]Astronomical Institute University of Bern (AIUB), Sidlerstrasse 5, 3012 Bern, Switzerland
[2]IMS Space Consultancy, ESA/ESOC, Robert-Bosch-Str 5, 64293 Darmstadt, Germany
[3]ESA/ESOC, Robert-Bosch-Str 5, 64293 Darmstadt, Germany
[*]Corresponding Author: benedikt.reihs@aiub.unibe.ch

**Abstract**

The surveillance of the region around the geosynchronous orbit (GSO) is usually done with optical sensors, i.e. telescopes. Placing a telescope on a satellite platform and performing the observations from space has several advantages, such as independence from weather and possibly an extended coverage. Several operational sensors of this type already exist, e.g. Sapphire and SBV. The European Space Agency is also supporting the development of technologies for such a mission. The envisaged mission design would be to place the sensor on a sun-synchronous orbit close to the terminator plane to observe objects in GSO passing through dedicated fences in the anti-solar direction.

In this work the correlation of tracklets is analysed, which means to test whether two tracklets originate from the same object. This is done by iterating on the hypothetical ranges and solving a boundary value problem. The results show that an initial catalogue build-up with observations only from such a sensor would be problematic because a large number of false associations is made. Even a post-processing technique based on the search for clusters in the correlations cannot reduce these false associations sufficiently. In total approx. 70% of the objects can be identified as unique clusters.

Other possible influences which are not investigated in detail is the seasonal dependence of the observations and the sensitivity of the correlation to higher noise levels of the sensor. It is concluded that a sensor used with the given mission design would probably be more useful for catalogue maintenance than for catalogue build-up. However, this also has to be seen in the framework of a complete surveillance network.

**Keywords:** space-based observations, correlation, space surveillance

## 1 Introduction

The importance of space surveillance is increasing with the number of space debris objects. Especially the geosynchronous orbit (GSO) including the important geostationary orbit (GEO) has seen an increase in objects due to e.g. multiple fragmentation events over the last years. The surveillance of the GSO is mainly done with ground-based telescopes from different sites and organisations. The main disadvantages of these sensors are that due to their co-rotation with the GSO, they have a limited coverage of the objects in this orbital regime and that the observations can be impacted by bad weather.

One possible way to overcome these problems is to place the telescope in space, which removes the effect of weather and depending on the orbit may also improve the coverage. There are already various examples for successful missions with space-based telescopes, such as e.g. Sapphire [1], SBV [2] and NEOSsat [3]. So far there is no European sensor, but the European

Space Agency (ESA) is conducting technological development studies for such a possible mission. The first feasibility analysis for this space-based optical (SBO) sensor was done by Flohrer et al. [4]. Recent ESA studies include the camera design [5], a possible mission design [6] and the development of an in-situ simulator of space-based measurements [7].

Within this framework, the research presented in this paper investigates the possibility to associate tracklets with each other and check if they originate from the same object. If this is the case, they are called to be correlated. This task is important for the initial catalogue build-up and inclusion of new objects. Different methods have been developed for this correlation task focussing on ground-based observations, see e.g. [8–10]. Only the work by Fujimoto et al. has also been specifically tested for a space-based observer [11].

For a space-based sensor, the overall performance and thus also the correlation capability is highly dependent on the mission design. As mentioned, here the current status of the ESA studies is used, which is explained in the following section.

## 2 Mission Design

The main idea of the mission design is to place the sensor on a platform in low Earth orbit (LEO), more specifically in a sun-synchronous polar orbit close to the terminator plane [4]. From there, GSO can be observed in the anti-solar (AS) direction and each GEO object passes through this area once per day. A tracking pattern has been designed which would allow it to create two leak-proof fences along GSO [6], assuming active pointing by a dedicated platform. The orbital elements of the platform are given in Table 1.

Table 1: Orbital elements of the observer platform at Feb 11, 2019, 18:00 UTC.

| | |
|---|---|
| Semi-major Axis, $a$ | 7128.0 km |
| Eccentricity, $e$ | 0.00001 |
| Inclination, $i$ | 98.39° |
| Right Ascension of the Ascending Node (RAAN), $\Omega$ | 74.04° |
| Argument of Perigee (AoP), $\omega$ | 0.0° |
| True Anomaly, $\varphi$ | 0.0° |

The geometry is sketched in Figure 1. The orbital plane is not exactly on the terminator plane, but slightly shifted to minimise the times when the view towards the two fences is blocked by the Earth. The angles to the fences are $\angle(AS, F1) = 9°$ and $\angle(F1, F2) = 22.5°$, which means that GEO objects need approx. 1.5 hours from the first fence to reach the second one for a follow-up observation. Due to the definition of the fences relative to the Earth shadow, their inertial direction is slowly changing over the year, but changes only marginally over a couple of days. Each fence has a width of 3°, but as a simplification no specific scanning strategy is used for the simulation of the measurements in this work. It is assumed that each object is detected once in the fence, which is simulated by a randomly selected start position within the 3°-stripe. The vertical extension of the fence is assumed to be sufficient to detect all objects with $i < 25°$. This is done in order to maximise the detections for the test of the correlation process. The investigation considering scanning and detections is not part of this work.

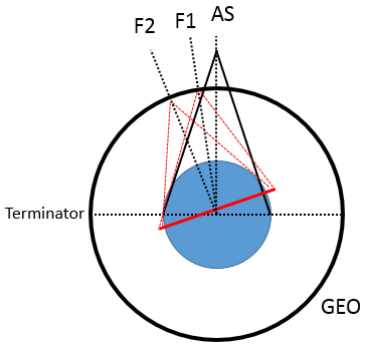


Figure 1: Sketch of the orbit (red) observing the two fences (F1, F2) which are defined relative to the anti-solar direction (AS).

This work does not discuss the sensitivity of the camera itself and thus the detectability of the object is purely based on an unobstructed view from the satellite to the fence. Based on the hardware requirements concerning e.g. pointing and exposure time, it is assumed that all tracklets have a length of 120 s, with a measurement point each 5 s. Gaussian white noise is added to the simulated measurements with $\sigma = 1$". The observables delivered by the telescope are the right ascension $\alpha$ and the declination $\delta$.

## 3 Correlation Method

### *3.1 Attributables*

The optical tracklets are fitted as attributables [12]. For ground-based measurements a simple linear fit may be used or a second-order, quadratic fit [13]. This decision mainly depends on the length of the tracklet and the observed variation therein. In the case of the space-based observer, the motion of the observing LEO satellite is a non-negligible influence during the measurement. For the fitting of the attributables, it has been

found that a third-order polynomial is giving bias-free estimates for the angular measurements $\alpha$ and $\delta$ including their derivatives and uncertainties:

$$\theta_{\alpha,\delta} = \bar{\theta}_{\alpha,\delta} + \dot{\bar{\theta}}_{\alpha,\delta} \cdot \Delta t + \frac{\ddot{\bar{\theta}}_{\alpha,\delta}}{2} \cdot \Delta t^2 + \frac{\dddot{\bar{\theta}}_{\alpha,\delta}}{6} \cdot \Delta t^3 \quad (1)$$

The fit is performed as a linear least squares with $\vec{\theta}_{\alpha,\delta} = \left[\bar{\theta}_{\alpha,\delta}, \dot{\bar{\theta}}_{\alpha,\delta}, \ddot{\bar{\theta}}_{\alpha,\delta}, \dddot{\bar{\theta}}_{\alpha,\delta}\right]$ as the parameter vector. The residuals of the fit are used to estimate the noise level of the observations and thus the uncertainty of the estimated parameters.

Additionally, Figure 2 and Figure 3 show the obtained values from the fitted attributables for the angles and angular rates, respectively. The circular structure in the data suggests that the measurements are dominated by the observer's dynamics, not only during the measurement of one tracklet but there is also a strong correlation between the two measured angles and even more for their angular rates for the overall set of observations.

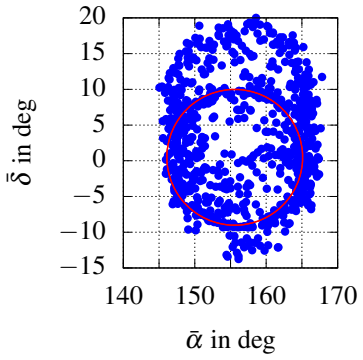


Figure 2: Distribution of the fitted angular observables $(\bar{\alpha}, \bar{\delta})$ over 48 hours.

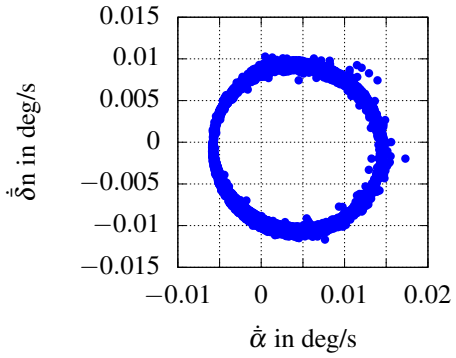


Figure 3: Distribution of the fitted angular rates $(\dot{\bar{\alpha}}, \dot{\bar{\delta}})$ over 48 hours.

In Figure 2, the red circle roughly indicates the region where objects exactly in GEO would be detected. The other detections belong to objects with an inclination $i > 0°$ and due to the characteristic relation in GEO between RAAN and inclination, these objects are detected above GEO for this time of the year and the current pointing direction. For the rates, the circular structure is much more clear, because it mainly results from the motion of the observer.

### *3.2 Association Method*

The association method used in this work is the boundary value approach by Siminski et al. [8], which was originally developed for the correlation of ground-based tracklets. The method uses the angles and angular rates from the attributable:

$$\mathscr{A} = \{\bar{\alpha}, \bar{\delta}, \dot{\bar{\alpha}}, \dot{\bar{\delta}}\} \, . \quad (2)$$

If a pair of attributables $\mathscr{A}_1$ and $\mathscr{A}_2$ is combined with two hypothetical ranges $\rho_1$ and $\rho_2$, two inertial positions can be calculated and used to obtain an initial orbit by solving Lambert's problem assuming Keplerian motion, see e.g. [14, 15]. For the resulting orbit the corresponding angular rates measured by the observer can be calculated and compared to the rates in the attributable. As a metric for the loss function, the Mahalanobis distance is used [16], which scales the differences $\vec{d}$ between the angular rates computed from the orbit and the one from the attributable by their summed uncertainties in the covariance matrix $C$:

$$M_d = \sqrt{\vec{d}^{\,T} \cdot C^{-1} \cdot \vec{d}} \, . \quad (3)$$

The covariance contains both the uncertainties of the measurements as well as the uncertainties from the initial orbit determination. A two-dimensional search for the minimum of the loss function in the $\rho_1$-$\rho_2$-space is performed using the BFGS-search [17]. An example of the loss function's topography is shown in Figure 4 for a specific number of revolutions between the tracklets. One clear minimum is visible and the topography seems to be smooth. The white areas indicate regions where no solution for a realistic earth-bound orbit can be obtained. As shown in the plot, this region can be large for the measurement geometry as described in this work, which can make the initialisation of the search more complex.

As mentioned, it also has to be considered that the number of revolutions is another unknown variable and the overall solution is selected as from the minima of each revolution.

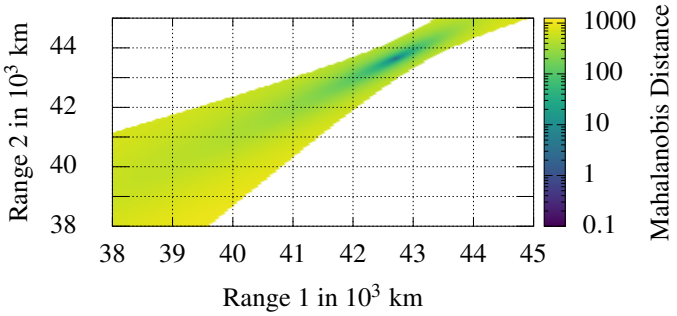


Figure 4: Example of the $M_d$ loss function for a pair of tracklets detected in the same fence after 24 hours.

### *3.3 Graph Theory Processing*

The pairwise correlation approach, although in general successful, can still contain a significant number of associations between tracklets which do not originate from the same object, called *false positives*. In order to reduce the number of false positives, a post-processing technique based on clustering of the pairwise correlations is applied. Yanez et al. [18] introduced a graph network for the identified correlations combined with an approach called Markov clustering. Here, a graph network is used as well being constructed of the tracklets as nodes and the identified correlations as edges connecting them. An example is shown in Figure 5. The identification of clusters is done by searching for triangles in the graph. The underlying idea is that if three tracklets all originate from the same object, they should also, ideally, be all correlated. In the example, there are four triangles, namely (A,B,C), (A,C,D), (A,B,D) and (B,C,D). The identification of such a triangle could also include the comparison of their orbits, which is not used in this work. After identifying the triangles, those which share a common edge, equal to two shared nodes, are merged into a common group. The example in Figure 5 would lead to one group of tracklets equivalent to one identified object. Afterwards, it is checked whether separate groups still share single nodes. The nodes are assigned to only one of the clusters using a greedy, non-iterative optimisation strategy with the aim to minimise the average Mahalanobis distance of the connections to the cluster. Due to its greedy nature, these splits can be non-deterministic if a node is part of multiple groups. However, the effect of this variation on the statistical results is rather low. It should again be mentioned that this post-processing technique is only dependent on the correlations and no combined orbital solutions are considered.

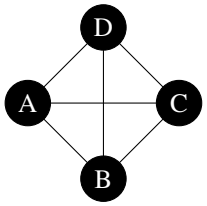


Figure 5: Example of a cluster in a graph network build from tracklets (A, B, C ,D) and the correlations between them.

## 4 Experiment

To test the correlation performance, a 48-hour measurement campaign by the SBO sensor has been simulated using approx. 1300 object in the geosynchronous region, here: 38000 km $< a <$ 46000 km, $e < 0.25$ and $i < 25°$. The simulation yields more than 5 000 tracklets in the two different fences, which coincides with the theoretically expected two detections per 24 hours on average. The simulation uses numerical propagation for all objects including a 16x16 gravitational field, luni-solar perturbations and solar radiation pressure (SRP).

In order to reduce the number of tested associations, the tracklet pairs are pre-filtered to allow only feasible combinations. For example, detections in the same fence which are less than 18 hours apart are not considered because of the minimum semi-major axis. To save further computation time, the restrictions are such that a correlation between the first detection in the first fence and the second detection in the second fence is not attempted. This reduces the overall number of available correlations, but due to the large number of objects and the regular observations there are enough correlations to get a significant result. This also challenges the post-processing approach because one possible correlation in the network will be missing by default.

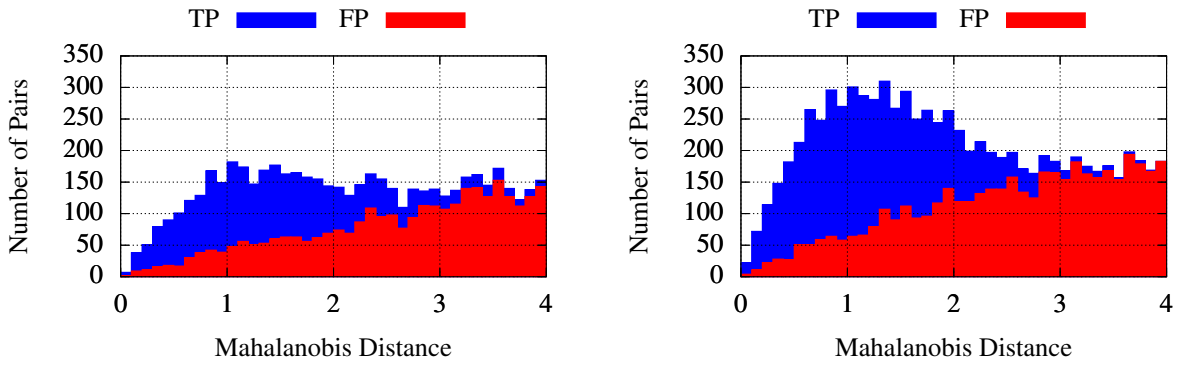


Figure 6: Distribution of Mahalanobis distances for true and false positives considering only tracklets which were detected in the same fence (left) or in different fences (right) before the post-processing.

The following results compare the numbers of *true positives* (TP) which are the correctly associated pairs of two tracklets from the same object and the already mentioned *false positives* (FP). As a first step the results without the graph network post-processing are shown. The first two plots separate the effects of the correlations in the same fence and in different fences, see Figure 6. It is visible that both cases have a large amount of false positives. In case of the correlations in the same fence, the peak due to the true positives is barely recognisable without the color coding. In contrast to that, the correlations from different fences have a much more pronounced peak, but it also has to be considered that on average there are three correlations in different fences and two correlations in the same fence available per object.

Combining these plots gives the overall result in Figure 7. Also here, it is clearly visible that the number of false positives is too high to have a reliable identification of objects. In order to reduce the number of false positives, the described post-processing technique is now applied to the data. The distribution of the remaining correlations is shown in Figure 8. A significant reduction in false positives could be achieved.

To compare the changes due to the post-processing in the numbers of the true and false positives, Figure 9 shows these total numbers for a threshold of $M_d = 4$. While the number of true correlations becomes only marginally smaller, the false positives are reduced to approx. one quarter of their initial value. In relation to the total number of correlations, before the post-processing 54% are FP which gets reduced to 24%. This value is still very large and indicates that there is still no reliable identification of objects possible.

However, the number of false positive correlations is not a good measure for the identification of objects after the clustering in the post-processing. Instead the groups which have been found as clusters are checked

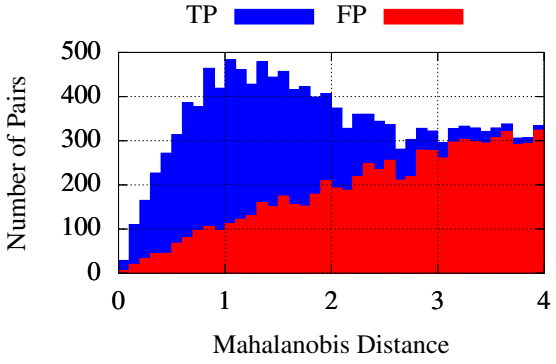


Figure 7: Distribution of Mahalanobis distances for true and false positives considering all pairs of tracklets before the post-processing.

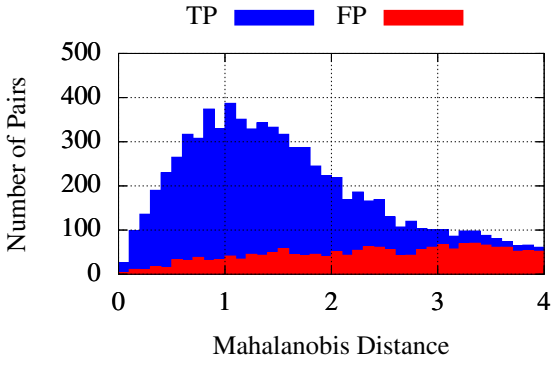


Figure 8: Distribution of Mahalanobis distances for true and false positives considering all pairs of tracklets after the post-processing.

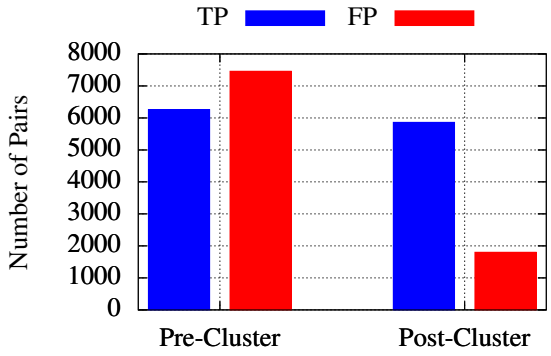


Figure 9: Comparison of the number of false and true positives before and after the post-processing for a threshold of $M_d = 4$.

whether they contain only tracklets belonging to the same object. Figure 10 shows the classification for all groups which contain at least three tracklets. A TP-group is a correctly identified object with all and only its own tracklets. The groups with FP contain mixtures of tracklets from different objects, whereas the FN groups do not contain all tracklets belonging to the main object in the cluster, which is the one with most tracklets. A group can be both FP and FN. The plot shows that approx. 900 objects form correct, separate clusters which is equivalent to approx. 70 % of the total objects in the simulation. This also shows that the large number of false positive correlations is mainly caused by a relatively small number of heavily connected groups, which contain 20-100 tracklets. That such a high number of tracklets cannot be due to a single object from a 48 hour campaign is obvious and thus, such a group could be rejected easily or used for further processing.

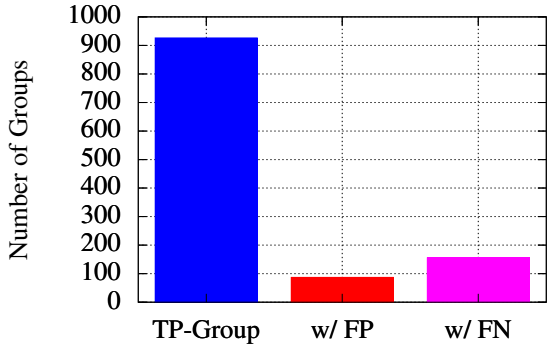


Figure 10: Comparison of the identified groups after the clustering analysis for a threshold of $M_d = 4$.

Concerning the post-processing, another possibility to reduce the false positives would be to have a more strict cut-off for the correlations which enter the graph. For example, the threshold could be reduced to $M_d = 3$, resulting in the number of true and false positives as shown in Figure 11. Although this means, that there may be less true positives, the percentage of false positives can be reduced to approx. 10% of the correlations. Interestingly, the classification of the groups does not change as much. This indicates that the majority of removed false positives is within the large cluster of mixed objects, which can still not be separated.

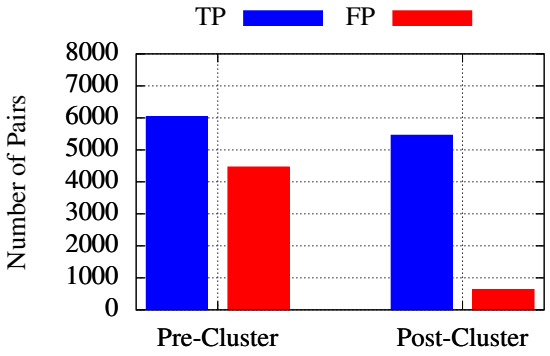


Figure 11: Comparison of the number of false and true positives before and after the post-processing for a threshold of $M_d = 3$.

Another interesting aspect in relation to this observation geometry is the accuracy of the determined orbits derived from detections in the same fence and detections in different fences. Figure 12 gives the standard deviations for the four slow-changing orbital elements excluding the argument of perigee due to the majority of near-circular orbits. They are calculated from the difference between the determined orbit and the reference orbit which was used for the simulation of the measurements. It can be seen that the semi-major axis is much more precise for the same fence case, because the object is detected twice roughly on the same position, which makes it easy to determine the orbital period compared to detections at different places. At the same time it becomes more problematic to estimate the orbital plane and the eccentricity. Thus the overall orbit quality from a single fence would probably be insufficient for a catalogue build-up. The inclination and RAAN is more precise if the measurements from two different fences are used and the uncertainty in the semi-major axis could be reduced in a cataloguing process by combining more observations. Due to the slow motion of the fences in inertial space, their width of 3° and the observer's motion, there is no common problem with singularities due to detections at exactly the same spot.

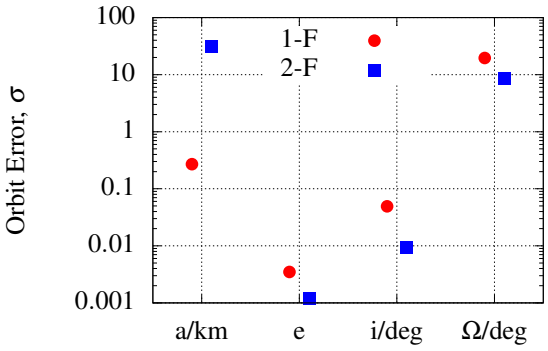


Figure 12: Comparison of the standard deviations of the orbit errors for pairs of tracklets from the same fence (1-F) and from different fences (2-F).

## 5 Discussion

One of the possible explanations for the large number of false positives is the reliance of the association decision on the angular rates, which are dominated by the observer satellite's motion, recalling Figure 3. Additional analyses has shown that the probability of having a false positive association is significantly higher for tracklet pairs which have the same observation geometry, i.e. a very similar observer position. Further insight could be gained by a comparison with a ground-based survey with a comparable scanning strategy. It remains likely that also other methods suffer from this issue, because all measurements are affected by it even if the association decision is based on different values.

Several other effects influence the correlation performance for such a mission, which have not been discussed in detail but should still be mentioned. First, the algorithm for the initial orbit determination does not include perturbations, which may be acceptable for short time frames like the 48 hours as presented here, but for longer times or high area-to-mass ratio objects which are strongly affected by SRP this might be more challenging.

The assumed sensor noise of 1 arcsecond is probably only realistic for a dedicated, large payload. A smaller demonstrator mission might not be able to reach this value. A larger noise level would increase the number of false positives even further and would be more demanding concerning the post-processing.

Due to the characteristic distribution of objects in GSO with regard to their relation between RAAN and inclination, there is also a seasonal dependence on the observations because the inertial pointing of the satellite towards its fences changes over the year. If one of the fences points at the dense region of ascending nodes, the observations will cluster even more and lead to more false positives.

## 6 Conclusion

To sum up the results in this work, it can be concluded that the association method is able to correlate observations from a space-based sensor. However, the design of the mission to build fences in GEO which are relatively stable over a short period of time leads to the problem that objects are detected multiple times at nearly the same position, which is probably the reason for the large number of false positives. The use of a post-processing method based on searching clusters within the correlated tracklets could reduce these false associations and identify a large share of the objects.

Other possible approaches could include a least squares orbit determination using the tracklets from an identified group with a residual analysis to confirm this object in the catalogue.

Based on the results here and considering that the sensor could have a higher noise level, it is questionable whether such a mission design would allow it to build-up a space object catalogue from scratch due to the problematic correlations for a significant part of the objects. If more than 48 hours of data is included, this could make it possible to distinguish more objects but at a significantly higher computational cost.

This leads to the conclusion that the space-based sensor as part of the mission as it is described here, is not ideal for unambiguous correlation and computationally efficient catalogue build-up. Additionally, such a sensor should also be considered in the context of an entire surveillance network and not only as a single sensor. One single ground-based telescope would not even be able to observe 70 % of the population in GSO within 48 hours. From this perspective, the impact of the SBO sensor is significant and a combination with a ground-based network can lead to a comprehensive surveillance system.

## Acknowledgements

The first author is supported by the European Space Agency through the Networking/Partnering Initiative.

## References

[1] A. Scott, J. Hackett, K. Man, On-orbit results for canada's sapphire optical payload, Advanced Maui Optical and Space Surveillance Technologies Maui (2013).

[2] J. Sharma, G. H. Stokes, C. von Braun, G. Zollinger, A. J. Wiseman, Toward operational space-based space surveillance, Lincoln Laboratory Journal, 13 (2002) 309–334.

[3] V Abbasi, S Thorsteinson, D Balam, et al., The NEOSSat Experience: 5 years in the life of Canada's space surveillance telescope, 1st NEO and Debris Detection Conference (2019).

[4] T. Flohrer, H. Krag, H. Klinkrad, T. Schildknecht, Feasibility of performing space surveillance tasks with a proposed space-based optical architecture, Advances in space research, 47 (2011) 1029–1042.

[5] J. Utzmann, A. Wagner, J. Silha, T. Schildknecht, P. Willemsen, F. Teston, T. Flohrer, A system design for space-based space surveillance, Proceedings of Small Satellites Systems and Services Symposium, 2014.

[6] J Utzmann, System Concept Report for SBSS Demonstrator System, ESA Study, ESA, 2013.

[7] J. Utzmann, L. Ferreira, G. Vives, L. Métrailler, N. Lièvre, T. Flohrer, Optical In-Situ Monitor–A Step towards European Space-Based Debris Observations, Advanced Maui Optical and Space Surveillance Technologies Conference, Maui, Hawaii, 2017.

[8] J. A. Siminski, O. Montenbruck, H. Fiedler, T. Schildknecht, Short-arc tracklet association for geostationary objects, Advances in space research, 53 (2014) 1184–1194.

[9] K. Fujimoto, D. J. Scheeres, J. Herzog, T. Schildknecht, Association of optical tracklets from a geosynchronous belt survey via the direct Bayesian admissible region approach, Advances in space research, 53 (2014) 295–308.

[10] D. Farnocchia, G. Tommei, A. Milani, A. Rossi, Innovative methods of correlation and orbit determination for space debris, Celestial Mechanics and Dynamical Astronomy, 107 (2010) 169–185.

[11] K. Fujimoto, D. J. Scheeres, Applications of the admissible region to space-based observations, Advances in Space Research, 52 (2013) 696–704.

[12] A. Milani, G. F. Gronchi, M. d. Vitturi, Z. Knežević, Orbit determination with very short arcs. I admissible regions, Celestial Mechanics and Dynamical Astronomy, 90 (2004) 57–85.

[13] J. M. Maruskin, D. J. Scheeres, K. T. Alfriend, Correlation of optical observations of objects in earth orbit, Journal of Guidance Control and Dynamics, 32 (2009) 194–209.

[14] R. Gooding, A procedure for the solution of Lambert's orbital boundary-value problem, Celestial Mechanics and Dynamical Astronomy, 48 (1990) 145–165.

[15] D. Izzo, Revisiting Lambert's problem, Celestial Mechanics and Dynamical Astronomy, 121 (2015) 1–15.

[16] P. Mahalanobis, On the generalised distance in statistics, Proceedings of the National Institute of Science of India, 2 (1936) 49–55.

[17] W. Press, Numerical recipes : the art of scientific computing, Cambridge University Press, Cambridge, UK New York, 2007.

[18] C. Yanez, J. C. Dolado Pérez, P. Richard, I. Llamas, L. Lapasset, Optical measurements association using optimized boundary value initial orbit determination coupled with Markov clustering algorithm, 7th European Conference on Space Debris, Presented paper, 2017.